



# The impact of water table fluctuation and salinity on LNAPL distribution and geochemical properties in the smear zone under completely anaerobic conditions

Reem Elfatih Ismail<sup>1</sup> · Riyadh I. Al-Raoush<sup>1</sup> · Motasem Y. D. Alazaiza<sup>2</sup>

Received: 26 December 2022 / Accepted: 8 July 2023 / Published online: 20 July 2023  
© The Author(s) 2023

## Abstract

Climate and groundwater are always in a state of dynamic equilibrium. Subsurface systems contaminated by light non-aqueous phase liquid (LNAPL) present a challenge to understand the overall impact of water table dynamics, due to various interacting mechanisms, including volatilization, and LNAPL mobilization/dissolution along the groundwater flow direction and oscillating redox conditions. We investigated the impact of water table fluctuations on LNAPL natural attenuation and soil geochemical characteristics in semi-arid coastal areas under saline conditions. Four soil columns operated for 151 days under anoxic conditions where a layer of benzene and toluene were subjected to a stable and fluctuating water table associated with low and high salinity conditions. The bottom of stable and fluctuating columns reached an anaerobic state after 40 days, while the middle of stable column took 60 days. pH values of the fluctuating columns covered a wide range, and at the end shifted towards alkaline conditions, unlike the stable columns. In fluctuating columns, pore water sulfate decreased in the middle, but in stable columns, it decreased in the first 40 days, which suggested that sulfate was the primary electron donor and sulfate-reducing bacteria were present. At the source zone, benzene and toluene reached their maximum concentration after 30 and 10 days for the stable and the fluctuating columns, respectively. Significant decrease in benzene and toluene concentrations occurred under the fluctuating water table. Salinity did not affect benzene and toluene concentrations in the aqueous phase, although water table fluctuations have the most effect. Soil solid-phase analysis shows fluctuating columns have less toluene than stable columns. Solid-phase analysis showed the fluctuating columns have less benzene and toluene concentrations as compared to the stable columns.

**Keywords** LNAPL · Water table fluctuations · Salinity · Arid region · Geochemical

## Introduction

Soil and groundwater contamination is considered a major environmental issue around the world where it adversely impacts groundwater quality, making it inadequate for human consumption and irrigation (Alazaiza et al. 2019, 2020; Chen et al. 2020; Huang et al. 2021; Mahmoudi et al. 2020). Non-aqueous phase liquids (NAPLs) have the

potential to remain in the subsurface for many years as a continuous source of groundwater contamination (Al-Raoush 2009, 2014; Kehew and Lynch 2011; Ning et al. 2018).

NAPLs are categorized into: light non-aqueous phase liquids (LNAPLs) with a density less than that of water and dense non-aqueous phase liquids (DNAPLs) with a density higher than that of water. The most common examples of LNAPLs are hydrocarbon fuel components, such as benzene, toluene, ethylbenzene and xylene. However, chlorinated solvents such as trichloroethylene (TCE) and tetrachloroethylene (PCE) are the most widespread DNAPLs (Cavelan et al. 2022). Mahmoudi et al. (2020) recently conducted a study on various types of pathogens, both natural and anthropogenic, which constitute another form of NAPLs that pose a threat to groundwater.

LNAPLs have been the focus of many studies due to their toxicity and longevity in the environment and

✉ Riyadh I. Al-Raoush  
riyadh@qu.edu.qa

<sup>1</sup> Department of Civil and Environmental Engineering,  
College of Engineering, Qatar University, PO Box 2713,  
Doha, Qatar

<sup>2</sup> Department of Civil and Environmental Engineering, College  
of Engineering, A'Sharqiyah University, 400 Ibra, Oman

the subsequent impact on human health (Gupta and Yadav 2017). Due to their complex interactions with geoenvironmental conditions, management and remediation activities of LNAPL-impacted sites are challenging in nature (Ebrahimi et al. 2019). When LNAPL is released into the subsurface, it migrates downward through the unsaturated zone under the influence of gravity until it reaches the water table, where it forms an LNAPL lens and spreads laterally while floating on the surface of the water table (Dobson et al. 2007; Jeong and Charbeneau 2014). On the other hand, DNAPL migrates downward through the vadose zone and continues its migration in the saturated zone under the influence of gravity until a low permeability barrier layer is encountered (Zheng et al. 2015). Water table level in hydrogeological systems fluctuates due to groundwater withdrawal, recharge, and seasonal variations in nearby water bodies, which in turn develops unique characteristics caused by the wetting and drying cycles that lead to variations in soil water content, redox conditions, biogeochemical properties (Haberer et al. 2012; Yang et al. 2017; Cavelan et al. 2022).

Water table fluctuations (WTF) have a significant impact on NAPL transport and spatial distribution within subsurface systems, particularly in the vertical direction (Lee et al. 2001a, b; Alazaiza et al. 2020; Van De Ven et al. 2021). WTF enhances mass transfer of oxygen from the atmosphere to the groundwater, which induces spatial and temporal variations in local redox conditions (Haberer et al. 2012; Rezan-ezhad et al. 2014; Zhou et al. 2015; Jia et al. 2017). When the water table falls, LNAPLs migrate downwards, leaving entrapped residuals in the unsaturated zone. The residual LNAPL partitions into solid, liquid, and vapor phases depending on the geochemical conditions and properties of subsurface systems (Reddi et al. 1998; Lee et al. 2001a, b; Kehew and Lynch 2011; Sookhak Lari et al. 2019; Alazaiza et al. 2020; Cavelan et al. 2022). On the other hand, when the water table rises, LNAPLs move upward along with the water table, which in turn induces LNAPLs redistribution upward in the unsaturated zone, leaving LNAPLs and air below the water table (Lee et al. 2001a, b; Dobson et al. 2007). The co-existence of entrapped LNAPLs and air in the saturated zone reduces the mobile free phase LNAPLs, which limits LNAPLs downward migration and enhances the dissolution and biodegradation of LNAPLs. Therefore, a zone of high residual phase concentration known as a smear zone could be developed due to vertical water table fluctuations in the presence of LNAPL (Kehew and Lynch 2011; Cavelan et al. 2022).

The impact of WTF on groundwater and soil contaminated with LNAPLs was monitored in the field (Teramoto and Chang 2017; Teramoto et al. 2020), studied experimentally (Dobson et al. 2007; Yang et al. 2017; Gupta et al. 2019; Alazaiza et al. 2020; Gupta and Yadav 2020; Van

De Ven et al. 2021) and numerically (Teramoto and Chang 2017; Sun et al. 2018; Huang et al. 2021).

Teramoto and Chang (2017) and Teramoto et al. (2020) monitored a contaminated site in Brazil and found that NAPL thickness is often lower during times of rising water levels and gradually rises during periods of low water levels. Dobson et al. (2007) found that WTF increased LNAPL dissolution and microbial activity compared with non-fluctuated model as measured by spatial distribution of electron acceptors and mass balances. Gupta et al. (2019) assessed the fate and transport of LNAPLs under different rates of WTF. The author emphasized the relationship between biodegradation rates and initial dissolved LNAPL concentrations. Alazaiza et al. (2020) utilized a simple image analysis technique (SIAM) to monitor LNAPL volumes at WTF sequences. Their study revealed that WTF has a considerable impact on the distribution of LNAPL. Van De Ven et al. (2021) observed the changes in the smear zone and mobile LNAPL thickness as a consequence of WTF. Sun et al. (2018) demonstrated in their experimental work that WTF induces dissolution of BTEX.

Similar studies were conducted to investigate biogeochemical properties in LNAPLs contaminated groundwater due to WTF (Lee et al. 2001a, b; Rühle et al. 2015; Zhou et al. 2015). Lee et al. (2001a, b) investigated petroleum hydrocarbons (PHCs) in a Korean sand aquifer. They found that water levels and subsurface hydrogeological properties affect contaminants distribution. Rühle et al. (2015) conducted column experiments and one-dimensional flow model to investigate the dynamics of the WT. Their research showed that while microbial activities differed across the stable and dynamic column, hydrogeological metrics showed no significant differences. Zhou et al. (2015) investigated TPH contaminated site and found that WTF altered groundwater microbial populations. Ulrich et al. (2009) claimed that the presence of salt in soil significantly impacted the bioremediation process of petroleum hydrocarbons. Another research stated that a decrease in salinity would improve the accessibility of soil organic matter to the soil microbial community (Qin et al. 2012).

While these studies provide valuable insights into the impact of WTF on NAPL-contaminated systems, the combined effects of WTF and salinity on natural attenuation of petroleum hydrocarbons and related changes in geochemical properties under anaerobic conditions have not been fully investigated and understood. Understanding this complex synergic behavior is crucial, especially in coastline regions where high salinity and accidental spills are common.

The main objective of this study was to investigate the impact of WTF and salinity on LNAPL distribution, mass removal, and changes of related geochemical properties in the smear zone under completely anaerobic reducing conditions. A series of controlled, automated soil column

experiments were conducted under stable and fluctuating water table regimes for 151 days. Experiments were conducted in closed systems to limit volatilization and aeration effects and to independently control the effects of WT dynamics. Benzene and toluene were used as a source zone of LNAPL under conditions of low and high salinity that represent brackish and seawater environments, respectively.

## Materials and methods

### Field sampling and soil analysis

Soil samples for all experiments were collected from the eastern coastline of Qatar (25° 34' 26.4" N 51° 29' 15.7" E). The site was selected because of its proximity to the Al-Shaheen oil field, where a continuous interaction between groundwater and seawater and tidal movements occurs, and basic soil analyses such as grain size distribution, hydrometer testing, and hydraulic conductivity were performed (Ngueleu et al. 2018, 2019).

Soil samples were collected between 10 and 50 cm below the ground surface. The samples were kept saturated with groundwater to preserve the soil's natural conditions. The soil was subsequently packed into the columns incrementally in 5 cm layers and compacted gently to ensure hydraulic continuity between the layers. Groundwater pH, electrical conductivity, and major cations and anions were measured using methods described in Ngueleu et al. (2019).

### Soil characterization

Soil samples were dried and then sieved using a series of sieves with varying mesh sizes between 0.063 and 13.5 mm. Figure 1 shows the grain size distribution curve using

Unified Soil Classification System (USCS). According to the USCS, the soil sample contained 6% of silt and clay particles, 45% of fine sand particles, 33% of medium sand particles, 11% of coarse sand particles, and 5% of fine gravel particles. Water content of the soil was 2% which is consistent with the (semi-) arid environmental conditions typically observed in Qatar. To analyze the soil elements, a destructive and non-destructive solid phase elemental analysis were performed. Two small samples were analyzed using a scanning electron microscope (SEM) coupled with an energy-dispersive X-ray spectrometer (EDS). The SEM images showed that the elemental composition of the soil was uniform, with Ca, Si, Mg, Al, Fe and Na being the most abundant elements, while K, S, and Mn were present in smaller quantities (Fig. 2). The results suggest that minerals like calcite, dolomite, and silica, which are commonly found in coastal or marine environments, may be present in the soil. Moreover, the destructive solid phase showed that, total sulphur was 2850 ppm, 0.07% dry for total nitrogen, and 10% dry for

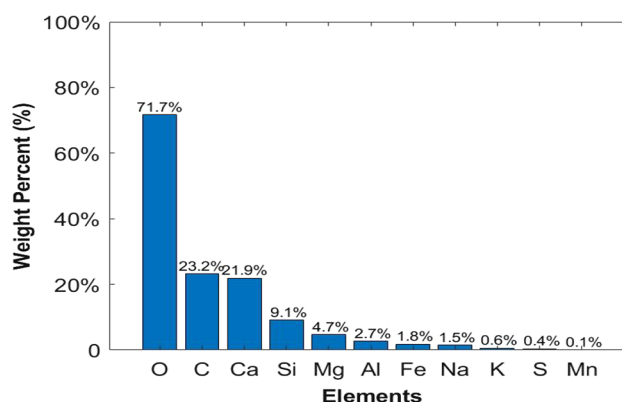
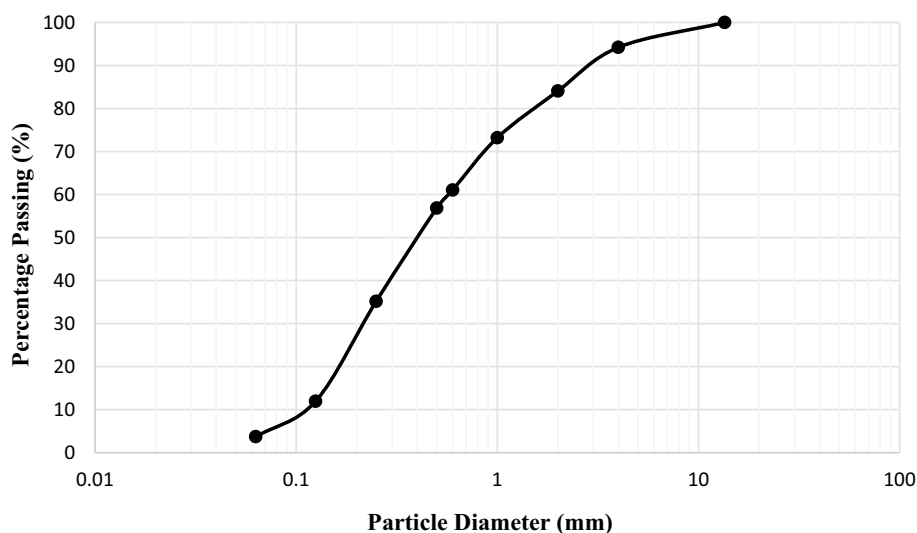


Fig. 2 Weight percentages of the elements detected in the solid phase of the soil

Fig. 1 Particle size distribution curve of the soil sample (USCS)



total carbon including 9.19% dry of inorganic carbon and 0.84% dry of organic carbon. The soil was assessed to determine its soluble salts content by simple solubilization with millipore water. Two samples of 30 g each of soil were used in two 60 mL glass bottles into which 46.5 mL of millipore water was later added, leaving no headspace in the bottles. The two bottles were agitated for 24 h on a tumbling wheel which rotated clockwise at a speed of 10 rounds per minute (rpm). Using electrodes connected to an advanced electrochemistry meter (Thermo Scientific, Orion Versastar), the average values from the two bottles were 7.7 for the pH and  $5730 \mu\text{S cm}^{-1}$  for the EC. Using an organic carbon analyzer and a nitrogen measuring unit, average values for DOC and TN were determined to be  $27.46 \text{ mg L}^{-1}$  and  $25.57 \text{ mg L}^{-1}$ , respectively. The organic matter in the soil was negligible.

Major cations concentrations were analyzed by inductively coupled plasma optical emission spectrometry. Average concentrations are  $632.71 \text{ mg L}^{-1}$ ,  $451.76 \text{ mg L}^{-1}$ , and  $562.83 \text{ mg L}^{-1}$  for Ca, Na, and S, respectively. Major anions concentrations were determined by ion chromatography (IC, Dionex ICS series). The average concentrations were  $1887 \text{ mg L}^{-1}$  for sulphate,  $758 \text{ mg L}^{-1}$  for chloride and  $86 \text{ mg L}^{-1}$  for nitrate. Overall, the results presented above are consistent with data from previous studies.

### Experimental setup of columns

Figure 3 shows a schematic diagram of the experimental setup. Each setup consisted of a pair of soil columns and an equilibrium column made of Teflon and Acrylic, respectively. Each column had a length of 60 cm, an inner diameter of 7.5 cm and a wall thickness of 0.6 cm.

The columns' tops and bottoms were sealed by caps and connected by three steel rods secured by bolts. A filter membrane (bubbling pressure of 600 mbar) was used to cover the top and bottom of the columns (Soil Measurement Systems, LLC, USA). The top and bottom caps had openings to supply and drain water from/to the columns. Water was supplied to the soil columns by connecting the soil column from the bottom to an equilibrium column by PVC 2-way valves connected by 15 cm of chemically resistant blue polyurethane tubing (Ark-Plas Products Inc, USA). The equilibrium column controls the level of water in the soil column. The top of each soil and equilibrium column was connected to a Tedlar bag, partially filled with argon gas, to prevent oxygen penetration into the columns. The system was completely sealed and operated under an anoxic condition where water/groundwater in storage Tedlar bags was purged by argon gas to reach dissolved oxygen (DO)  $< 0.8 \text{ mg L}^{-1}$ .

Each soil column equipped with 4 ports (1/800 NPT compression fittings) along its sides at 10, 20, 30, and 50 cm below the top of the column. The 20 cm port was tightened and fitted with Teflon septa and used only for injection of NAPLs. The other three ports have filtration screens to prevent soil washout. All ports were fitted with 1/8—27 NPT thread with 7/16" Hex to classic series Barb, 1/8" ID tubing, and white Nylon, and connected with 10 cm of chemically resistant polyurethane tubing for collecting aqueous samples. A nine-channel pump (Tower II pump, CAT. M. Zipperer, GmbH, Germany) was used to control water level fluctuation by pumping water to the Tedlar bag linked to the equilibrium columns and served as a water reservoir. Each channel of the pump was operated individually with the design flow rate.

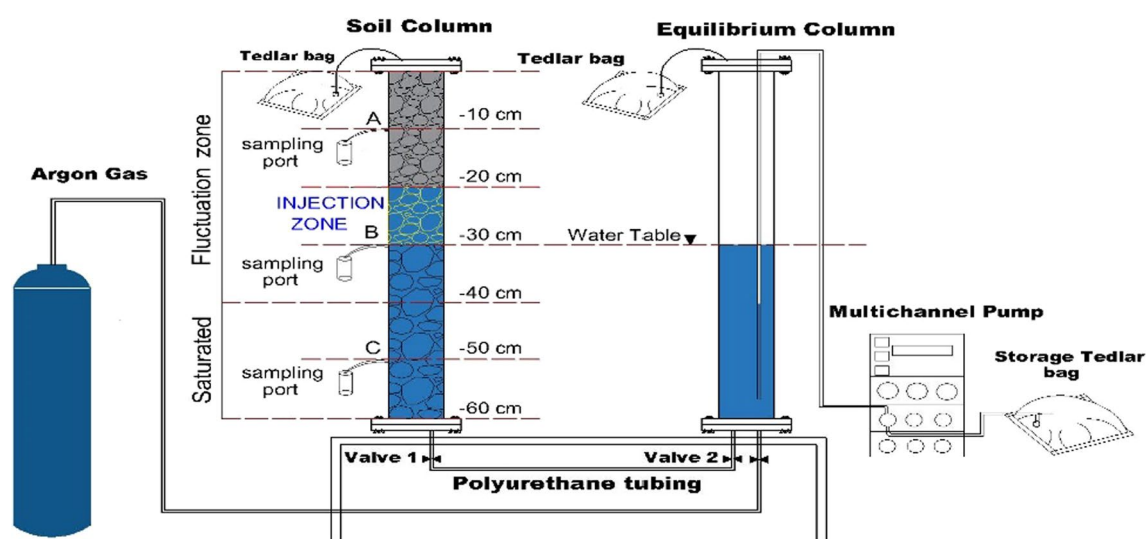


**Fig. 3** Schematic diagram of the experimental setup. Depth A (− 10 cm), depth B (− 30 cm), and depth C (− 50 cm) from the top of the column

## Experimental procedure

Four pairs of soil and equilibrium columns were used to investigate the synergic impact of WTF and salinity on the attenuation and distribution of LNAPLs in the smear zone. Two soil columns were allocated for stable water level conditions (labeled as S1 and S2) whereas the other two soil columns were allocated for fluctuating water level conditions (labeled as F1 and F2). Brackish water ( $\sim 4000 \mu\text{S cm}^{-1}$ ) was used in S1 and F1 soil columns whereas high salinity water ( $\sim 25,000 \mu\text{S cm}^{-1}$ ) was used in S2 and F2 soil columns.

Benzene ( $\text{C}_6\text{H}_6$ ) and toluene ( $\text{C}_7\text{H}_8$ ) were used as LNAPLs as these compounds can be commonly found in seawater in the vicinity of natural gas and petroleum deposits. Al-Ghouti et al. (2019) found that raw produced water collected from a natural gas field in Qatar contains 21 and  $3.8 \text{ mg L}^{-1}$  of benzene and toluene, respectively. The density and solubility in water of benzene at  $25^\circ\text{C}$  were  $0.874 \text{ g cm}^{-3}$  and  $1800 \text{ mg L}^{-1}$ , whereas toluene is  $0.867 \text{ g cm}^{-3}$  and  $520 \text{ mg L}^{-1}$ , respectively (Ruffino and Zanetti 2009). Salinities of  $4000 \mu\text{S cm}^{-1}$  and  $25,000 \mu\text{S cm}^{-1}$  were used to represent brackish and seawater conditions at the sampling location, respectively (Ngueleu et al. 2018, 2019). Prior to starting the experiments, soil columns were saturated with an anoxic synthetic solution with  $\text{DO} < 0.8 \text{ mg L}^{-1}$  to mimic natural groundwater (Ngueleu et al. 2019). Table 1 summarizes the properties of the synthetic groundwater.

Soil columns were then saturated and drained four times to develop the anaerobic conditions in the columns (i.e., to preserve reducing conditions of the natural soil). To prepare the columns for benzene and toluene injection, the water level was fixed at  $-25 \text{ cm}$  (considering the top of the soil columns as reference). LNAPLs were injected with an airtight glass syringe equipped with a stainless-steel needle. At  $-20 \text{ cm}$  depth,  $5 \text{ mL}$  of liquid benzene ( $99.9 + \%$ , Sigma-Aldrich, Canada), and  $5 \text{ mL}$  of liquid toluene ( $99.9 + \%$ ,

Sigma-Aldrich, Canada) were injected. In soil columns, water levels fluctuated between the top of the column and  $-40 \text{ cm}$ . Each drainage-imbibition cycle lasted four days, allowing  $6\text{--}12 \text{ h}$  for equilibrium. The flow rate in upward and downward directions was approximately  $0.407 \text{ mL min}^{-1}$  to mimic natural conditions in the sampled location (Baalousha 2016). The experiment ran for 151 days at a room temperature of  $(22 \pm 2^\circ\text{C})$ . To ensure that oxygen ( $\text{O}_2$ ) does not penetrate the system, equilibrium columns were purged with argon (Ar) gas as needed. Aqueous samples were collected from soil columns at stable conditions every 4 days from the middle of the column (i.e., port B at depth of  $-30 \text{ cm}$ ) and biweekly from the top of the column (i.e., port A at depth of  $-10 \text{ cm}$ ) and bottom of the column (i.e., port C at depth of  $-50 \text{ cm}$ ). Whereas, for the fluctuating columns at the time of saturation, aqueous samples were collected every  $8\text{--}10$  days from the middle of the column (depth B) and bottom of the column (depth C) and biweekly from the top of the column (depth A). At the time of drainage, aqueous samples were only collected from the bottom (depth C).

## Analytical methods

Samples were collected from the stable and the fluctuated columns every 4 days. Aqueous samples were collected for the measurements of concentrations of benzene, toluene and sulfate. In addition, ion chemistry (IC), dissolved inorganic carbon (DIC), dissolved oxygen (DO), redox potential (ORP), pH, and Electrical Conductivity (EC) were measured.

At the end of the experiment, all soil columns were fully drained and disassembled to measure the final concentrations of toluene and benzene in the soil by GC-MS. Soil samples were obtained from the top of the soil columns using a hand hammer, and column was divided into several layers with a thickness of  $10 \text{ cm}$ . A total of  $15 \text{ g}$  of homogenized soil was collected in three separate vials from each part. Trace elements such as Si, Fe, Mg, and S were measured using [Energy Dispersive-X-Ray Fluorescence spectrometry, ED-XRF (S2 PUMA analyzer, Bruker, Germany)]. Two samples were collected from the soil before the start of the experiment, and at the end, each column was sliced into 6 parts, and three samples ( $10 \text{ g}$  each) from each slice were collected and analyzed.

Eh, pH, DO, and EC were measured using an Orion™ Versa Star Pro™ Benchtop Meter (Thermo Scientific) immediately after collecting the aqueous samples to prevent the effects of degassing or reactions caused by oxygen ingress. A 850 Professional Ion Chromatography (Metrohm) equipped with two conductivity detectors was used to measure the concentrations of anions, whereas Metrosep C4 150/4.0 column with a  $10 \mu\text{L}$  sampling size was used to measure the

**Table 1** Synthetic groundwater properties

| Parameter                                | Value  |
|--|--|
| pH                                       | $\sim 7.5$   |
| Temperature                              | $22 \pm 2^\circ\text{C}$   |
| $\text{MgCl}_2$                          | $89 \text{ mg L}^{-1}$   |
| KCl                                      | $24 \text{ mg L}^{-1}$   |
| $\text{CaCl}_2 \cdot \text{H}_2\text{O}$ | $245 \text{ mg L}^{-1}$  |
| NaCl                                     | $1300 \text{ mg L}^{-1}$<br>(low salinity— $4000 \mu\text{S cm}^{-1}$ )      |
| NaCl                                     | $20,000 \text{ mg L}^{-1}$<br>(high salinity— $25,000 \mu\text{S cm}^{-1}$ ) |
| DO                                       | $< 0.8 \text{ mg L}^{-1}$  |



cations. Data from ion chromatography was processed using MagIC Net software.

Gas chromatography–flame ionization detector (Clarus 680, Perkin Elmer, USA) was used for the measurements of organic concentrations from aqueous samples. DIC/DOC concentrations were measured using a total organic carbon analyser (SKALAR, Formacs HT/TN TOC/TN Analyzer, Netherland). Each sample was analyzed three times and the average value was reported. More details about the analytical methods can be found in the supplementary materials section.

## Results and discussion

### Pore water geochemistry

Prior to the start of the experiments, the porosity of the packed soil in the four soil columns was determined by the volumetric method. The porosity of the soil in the stable water level columns, S1, and S2, was 22% and 23%, respectively. Whereas the porosity of the fluctuated water level columns, F1, and F2, was 24% and 26%, respectively. Differences in the porosities between the four columns are mainly due to the manual compaction of the soil in the columns.

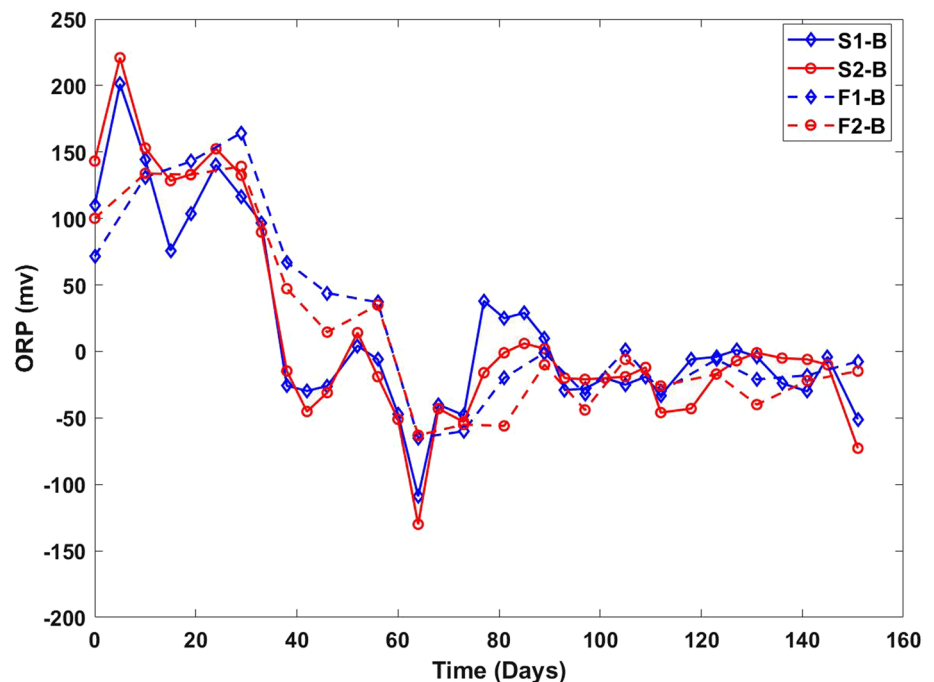
### Water table and redox regimes

Figure 4 shows the ORP for all soil columns. ORP indicates the ability of a given chemical to oxidize or reduce another chemical (Meng et al. 2021). Natural water chemistry is

influenced by redox processes, which influence the mobility and availability of a wide range of inorganic and organic species (Ramesh Kumar and Riyazuddin 2012). The redox potential is an important factor for characterizing organic-rich contamination plumes as bacteria get energy by oxidizing organic carbon and reducing terminal electron acceptors (Abbas et al. 2017; Zhang and Furman 2021). Several factors, including electro-redox components and soil organic matter and bacterial biodegradation, can impact redox potential (Naudet et al. 2004). The influence of WTF at a given salinity can be observed by comparing stable and fluctuation columns. At low salinity conditions (i.e., S1 and F1), the  $p$  value for S1 and F1 is  $0.6319 > 0.05$ , indicating that there are no significant differences between the stable and the fluctuating columns. In the middle of the columns (depth B), measured ORP values at the start of the experiment were 100 and 60 mV for the columns S1 and F1, respectively. 40 days after LNAPLs injection, ORP values decreased and ranged between  $-40$  and  $40$  mV at depth B in S1 and F1, respectively. The ORP values in the middle of the stable column S1 are lower than those in the fluctuated column F1, which can be attributed to the presence of more concentrated contamination in the stable column than in the fluctuated column which decreased due to fluctuated water table (Feisthauer et al. 2012; Khan et al. 2018).

At high salinity conditions (i.e., S2 and F2), the  $p$  value for S1 and F1 is  $0.9028 > 0.05$ , indicating that there are no significant differences between the stable and the fluctuating columns due to the influence of water table fluctuation. The initial ORP values were 140 and 100 mV at the middle of the columns S2 and F2, respectively. 40 days after

**Fig. 4** Oxidation–reduction potential (ORP) at depth B for the columns S1 and F1 (for the case of low salinity columns), and the columns S2 and F2 (for the case of high salinity columns)



LNAPLs injection, ORP values decreased where values ranged between  $-50$  and  $20$  mV in the middle of S2 and F2, respectively. Similar to the low salinity column F1, ORP values at the middle of the fluctuating column F2 are slightly higher than the middle of the stable column S2 and the same explanation can be applied.

The influence of salinity can be observed by comparing stable columns (i.e., S1 and S2,  $p$  value =  $0.8972 > 0.05$ ) and fluctuating columns (i.e., F1 and F2,  $p$  value =  $0.2843 > 0.05$ ). The  $p$  value indicating that there are no significant differences between the ORP values at stable and the fluctuating columns of different salinities. For the stable columns, 40 days after LNAPLs injection, ORP values decreased and ranged between  $-40$  and  $-50$  mV at the middle of the columns S1 and S2, respectively. Whereas after 60 days, values of ORP in both columns reached  $-150$ . Salinity didn't affect ORP between the two stable columns. Similarly, for the fluctuating columns with different salinities (i.e., F1 and F2), ORP values in the middle were  $\sim 50$  and  $100$  mV for F1 and F2, respectively. By the third imbibition cycle, ORP values increased to  $\sim 150$  mV in both F1 and F2, then decreased to  $-50$  mV after 60 days. The ORP values at the middle of the fluctuating columns are slightly higher than in the stable columns.

To summarize ORP results, the same pattern was observed in the middle of the stable and the fluctuating columns in all experimental conditions (i.e., low and high salinity) where ORP values reach the anaerobic condition. In a manner similar to that, Shafieiyoun et al., (2020a, b) conducted an experiment where using biocide in one of the reactors, Eh values didn't change during the experiment, while for the brackish water and high salinity reactors, Eh values after 40 days dropped to  $< +300$  mV (equivalent to  $100$  mV for ORP).

Data show that the WTF has more profound impact on ORP than salinity. ORP values indicate that anaerobic conditions were developed in all soil columns (Ismail et al. 2020; Shafieiyoun et al. 2020a, b; Meng et al. 2021). According to the classification of Reddy and DeLaune (2008) and Zhang and Furman (2021), soil columns were under aerobic conditions for the first 10 days, weakly reducing conditions were observed in all columns after 40 days from the start of the experiments, except at the middle of the fluctuating columns, and moderate reducing conditions were observed in all columns after 60 days. Figure 4 shows that there is no significant difference in ORP values in stable water level conditions at different salinities (i.e., S1 and S2). However, in fluctuated systems, ORP values decreased during water level rise and increased again during water level fall which is consistent with observations of Rezanezhad et al. (2014).

ORP values indicate that the development of anaerobic conditions was slower in the middle part of fluctuating water levels where anaerobic conditions were developed

after 60 days. However, faster anaerobic was reached in the middle of the stable columns. This observation can be attributed to the rise and dropping of WT which can results in entrapped air in the middle of the columns (Rezanezhad et al. 2014; Meng et al. 2021). Rezanezhad et al. (2014) found that oxidizing conditions formed in the center of the fluctuating soil column after each drainage phase, and Eh values increased from  $-100$  to  $+700$  mV due to oxygen penetration. In this experiment, ORP values in the fluctuating water table columns did not increase significantly as the experiment was performed under controlled anaerobic condition.

This observation suggested that microbial activity and anaerobic degradation were less improved in the middle of the fluctuating column. The higher ORP at the middle of the fluctuating columns could also be attributed to the effect of the presence of LNAPL as a source zone combined with the WTF that influences organic concentrations and redox conditions (Lueders 2017; Ning et al. 2018). In previous studies, Vincent et al. (2011), Khan et al. (2018) and Logeshwaran et al. (2018) found that the presence of organics in the soil has an adverse effect on the development of the microbial community.

### Concentration of electron acceptors

To sustain the microorganism's living and growth, they strive for energy from the available electron donors and acceptors. DO produces the greatest amount of energy from organic carbon oxidation of any commonly available electron acceptor, oxygen-reducing microorganisms will compete for the available electron in DO, and the reaction will continue until DO is depleted. The sequence of electron acceptor utilization is often predictable in the order of  $O_2 > NO_3^- > Mn^{4+} > Fe^{3+} > SO_4^{2-} > CO_2$  (Borch et al. 2010; McMahon et al. 2011; Laverman et al. 2012; Ohio EPA 2014). In this experiment, DO was minimized by purging by argon gas for the duration of the experiment (Ngueleu et al. 2019; Shafieiyoun et al. 2020a, b). Measuring biodegradation can be determined by the removal of electron donors (i.e., benzene and toluene) or electron acceptors (i.e., nitrate and sulfate) (Chapelle et al. 1996; Borch et al. 2010; McMahon et al. 2011; Ohio EPA 2014).

Ion chromatography (IC) was used for the measurement of cations and anions. The IC results indicated that an aqueous phase of iron (Fe), manganese (Mn), sulfur (S), and nitrogen (N) were available in the system. It was also observed that aqueous nitrate ( $NO_3^-$ ) concentration was detected at the top, middle and bottom of all soil columns. During the first 30 days, the concentration of  $NO_3^-$  was in the range of  $2$  and  $5$  mg  $L^{-1}$  at the middle (i.e., depth B) of the stable columns (i.e., S1 and S2). For the fluctuating columns (i.e., F1 and F2),  $NO_3^-$  was only detected in the middle

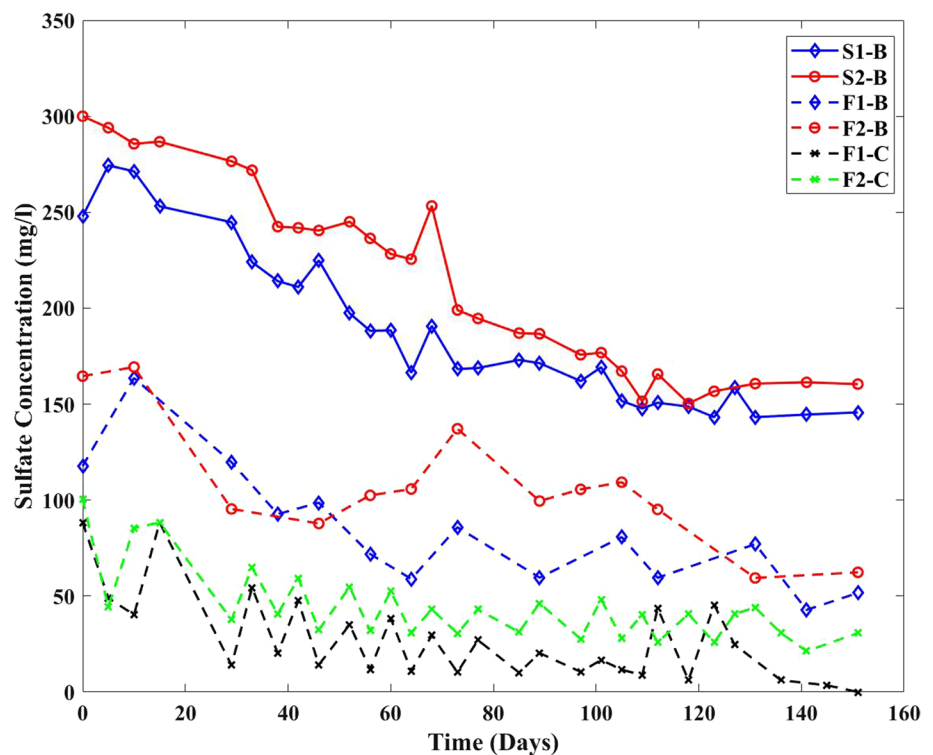
of the column in the range of 1 and 5 mg L<sup>-1</sup> in the first 60 days. Detection of NO<sub>3</sub><sup>-</sup> corresponds to oxygen decrease to less than 0.8 mg L<sup>-1</sup> and the development of the anaerobic condition as supported by ORP values given in Fig. 4. The aqueous Mn concentration was detected in the middle of the columns S1 and S2 in the range of 6 and 13 µg L<sup>-1</sup>, respectively until day 100. while, for the fluctuating columns F1 and F2 were observed in the first 15 days in the middle of the columns in the range of 1 and 23 µg L<sup>-1</sup>, respectively. The ferric iron was detected in the middle of the stable columns (i.e., S1 and S2) in the range of 7 and 14 µg L<sup>-1</sup>, while for the fluctuating water level columns (i.e., F1 and F2), the concentration in the middle was detected after 15 days and ranged between 4 and 7 µg L<sup>-1</sup>, respectively. Both Fe and Mn become under detected limit after 30 and 100 days for the fluctuating and stable columns, respectively. Moreover, in an experiment similar to this, Rezanezhad et al. (2014) found that the mid-section of the columns, where the discrepancy in redox conditions is greatest, there is a significant difference in the pore water distributions of redox-sensitive elements (Fe, Mn, P, S). Fe and Mn can be used as electron acceptors by microorganism to reduce toluene and benzene in this section of the columns. Greskowiak et al. (2005) in his work noticed that the decrease of Fe concentrations began along with the decrease in Mn concentration, which can be the case here.

Unlike the previously mentioned electron acceptors, the aqueous sulfur concentrations were detected in the columns at all depths in the range of 300–88 mg L<sup>-1</sup>. Low nitrate,

manganese and iron concentrations reveal that denitrification, manganese and iron decrease were not the dominant biodegradation processes, however, sulfate-reducing bacteria (SBR) are expected to be the dominant (Davis et al. 1999; Anneser et al. 2008). The decrease in sulfate concentration was thought to be a key mechanism regulating anaerobic biodegradation in polluted aquifers (Feisthauer et al. 2012).

As shown in Fig. 5, the influence of WTF at a given salinity was observed by comparing stable and fluctuation columns (i.e., S and F). For the low salinity columns (i.e., S1 and F1), the  $p$  value =  $5.6633e^{-7} < 0.05$  implying that there is a statistical difference between sulfate concentrations in the middle of the two columns. The initial sulfate concentrations were 250 and 110 mg L<sup>-1</sup>, for S1 and F1, respectively. 10 days after the injection of LNAPLs, sulfate concentrations increased to 270 and 170 mg L<sup>-1</sup>, respectively, then continued to decrease to 145 and 60 mg L<sup>-1</sup>, respectively, by the end of experiments. The increase in concentration that occurred at the beginning of the experiment could be a result of the movement of water to the top of the column which carry sulfate ion along the column. It was observed that for S1 and F1, the concentration of sulfate was significantly decreased during the experiment. The decrease in the stable column can be attributed to the development of sulfate-reducing bacteria (Shafieiyoun et al. 2020a, b). Moreover, the decrease in sulfate concentration during the experiment coupled with ORP reduction might be an indication of toluene and benzene degradation by the SBR (Anneser et al. 2008; Huang et al. 2016; Shafieiyoun

**Fig. 5** Dissolved sulfate concentrations at depth B of the stable columns, and depth B, and C for the fluctuating columns





et al. 2020a, b; Wei et al. 2018). For the fluctuating column, at 40 days from the start of the experiment, a smell of rotten egg was noticed during sampling at the bottom of the fluctuating columns. This observation is consistent with the observations of Sherry et al. (2013) and Müller et al. (2017) implies that the decrease in sulfate concentration which used as a terminal electron acceptor would result in the production of hydrogen sulfide ( $H_2S$ ).

In high salinity columns (i.e., S2 and F2), the  $p$  value =  $2.5165 \times 10^{-6} < 0.05$  which indicates that there is a statistical difference between sulfate concentrations in the middle of the two columns. The initial pore water sulfate concentrations were 300 and 160  $mg\ L^{-1}$ , for the middle of S2 and F2, respectively. For S2, sulfate concentration decreased to reach 160  $mg\ L^{-1}$  by the end of the experiment, while for F2, sulfate concentrations decreased and reached 50  $mg\ L^{-1}$  by the end of experiment. Same as for the low salinity stable column, sulfate concentration decrease can be attributed to the development of sulfate-reducing bacteria which coupled with ORP reduction. For the fluctuating column, unlike the low salinity column, no smell of rotten egg was observed which may indicate that extremely high salinity may act as a natural barrier to the metabolism of hydrocarbons (Sei and Fathepure 2009).

The influence of salinity was observed by comparing stable columns (i.e., S1 and S2,  $p$  value =  $0.0312 < 0.05$ ) and fluctuating columns (i.e., F1 and F2,  $p$  value =  $0.0415 < 0.05$ ). The aqueous sulfate concentrations at the middle of the two stable columns followed the same trend during the

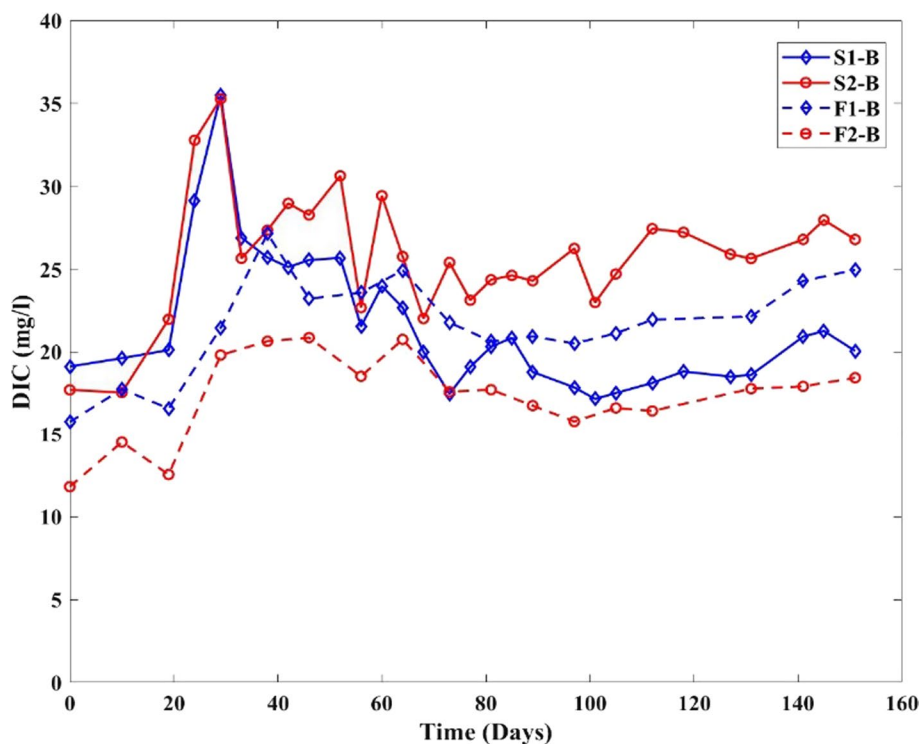
experiment. A decrease in sulfate concentrations occurred in the middle of the columns. It was observed that concentrations at all depths in column S2 are higher than in S1. The decrease in sulfate concentrations can be linked to the degradation of toluene and benzene. This observation can be supported by looking at the concentrations of non sensitive redox parameters such as the concentrations of  $Ca^{+}$  (Supplementary materials).

In the fluctuating columns (i.e., F1 and F2,  $p$  value =  $0.0415 < 0.05$ ), sulfate concentrations followed the same trend at all locations (i.e., depth B and depth C). At the middle, sulfate concentrations decreased for both columns and the values fluctuated during wetting and drying cycles that enhanced redox conditions. Sulfate concentrations at the bottom of the columns were significantly lower than those in the middle of the columns. This observation can be attributed to the dissolution of sulfate as a result of the admixing more diluted water from the equilibrium columns (Rezanezhad et al. 2014). The concentrations of sulfate at the bottom of the fluctuating column is different from the stable column, the changes in elemental distributions can be seen in the fluctuation due to physical movement caused by the rising and falling of the water table (Rezanezhad et al. 2014).

### Dissolved inorganic carbon (DIC)

DIC concentration is an indicator of the mineralization of NAPL. Figure 6 shows the concentrations of DIC measured at the middle of stable and fluctuating soil columns.

**Fig. 6** Dissolved inorganic carbon (DIC) concentrations at depth B for stable and fluctuation columns



The influence of WTF was observed by comparing the low salinity columns (i.e., S1 and F2) and the high salinity columns (i.e., S2 and F2). For the low salinity columns ( $p$  values =  $0.0343 < 0.05$ ), the initial DIC concentrations at the middle were 19 and 16 mg L<sup>-1</sup> for S1 and F1, respectively. DIC was increased to 35 and 27 mg L<sup>-1</sup> after 30 and 40 days, respectively. The increase in DIC values is consistent with the start of the reducing conditions in the columns (Fig. 4). For the high salinity columns (i.e., S2 and F2,  $p$  values =  $3.5738 \times 10^{-10} < 0.05$ ), the initial DIC concentrations at the middle were 17 and 11 mg L<sup>-1</sup>, respectively. However, DIC was increased to 35 and 20 mg L<sup>-1</sup> for S2 and F2 after 30 and 40 days, respectively.

The influence of salinity was observed by comparing stable columns (i.e., S1 and S2,  $p$  values =  $9.4813 \times 10^{-5} < 0.05$ ) and fluctuating columns (i.e., F1 and F2,  $p$  values =  $2.6575 \times 10^{-9} < 0.05$ ). The statistical  $p$  values showed that DIC for both the stable and fluctuating columns are statistically different. In columns S1 and S2, DIC values followed the same trend where values increased as anaerobic conditions developed in the columns and then decreased and fluctuated between 20 and 25 mg L<sup>-1</sup>. DIC values in column S2 were slightly higher than S1, which can be attributed to the effect of salinity.

DIC concentrations in columns F1 and F2 followed the same trend throughout the experiments where concentrations increased to 27 and 20 mg L<sup>-1</sup>, respectively. DIC values imply that mineralization was developed in the middle of columns where LNAPLs were injected. In stable columns, the increase in DIC is more in the column S2 whereas in fluctuating columns, DIC is more in F1. These observations are consistent with the suggestions of Kehew and Lynch (2011), Wei et al. (2018) and Wurgaft et al. (2019).

### Concentration of dissolved organics

Transport of petroleum hydrocarbons in soil is influenced by various factors, including the water velocity gradient, hydraulic conductivity, intensity of evaporation and transpiration, density gradient, seasonal changes in water surface level, and diffusivity (Farahani and Mahmoudi 2018). Such factors enhance the decrease in the concentrations of these contaminants by the natural attenuation processes which includes volatilization, dilution and dispersion, sorption to soil particles, and biodegradation (Kehew and Lynch 2011; Yang et al. 2017; Hatipoğlu-Bağcı and Motz 2019). Depending on their solubility and other conditions, toluene and benzene will progressively dissolve into the aqueous phase and move in dissolved form in the groundwater flow system (Kehew and Lynch 2011). Throughout the experiments, toluene and benzene were under saturated conditions in the stable columns and continuously under cycles of saturated and unsaturated conditions in the fluctuating columns. This

in turn led to the development of three distinct states as free, dissolved, and residual phase (Yang et al. 2017).

### Concentration of dissolved and solid-phase toluene

Dissolved toluene concentrations are presented in Fig. 7a–c. In low salinity columns (i.e., S1 and F1), the initial toluene concentrations at the top, middle and bottom were 42, 179, and 0 mg L<sup>-1</sup>, and 70, 73, and 0 mg L<sup>-1</sup> in S1 and F1, respectively. The concentration of toluene was the highest at the middle of the columns where the source zone exists. As WT rises, it pushes toluene to the top of the column and a new smear zone was developed (Dobson et al. 2007; Van De Ven et al. 2021). Toluene is known as the easiest of the BTEX compounds to breakdown (Foght 2008; Phelps and Young 1999). For the top of S1 and F1 ( $p$  value =  $0.0012 < 0.05$ ). At the top of the S1, slight change in toluene concentration was observed after 80 days following the injection, whereas in column F1, concentrations increased to a maximum value of 160 mg L<sup>-1</sup> by the third saturation cycle. The increase in concentration in F1 resulted from the movement of toluene from the source zone where it was injected at (– 20 cm) to the top of the column at the time of imbibition cycle. Thereafter, the concentration declined until it reached 33 mg L<sup>-1</sup> by the end of the experiment. The fluctuations of water table are the main cause of mass transfer which caused the redistribution of toluene and the change in toluene concentrations at the top (depth A) of the column.

For the middle of the columns (S1 and F1), at the middle of S1, the concentration at S1 increased to a maximum value of 200 mg L<sup>-1</sup> after 29 days. Whereas in F1, a maximum concentration of 160 mg L<sup>-1</sup> was reached after 10 days following toluene injection (i.e., the second saturation cycle). The statistical analysis of the concentrations showed that  $p$  value  $8.53 \times 10^{-15} < 0.05$  which implies that there are statistical differences between toluene concentrations at the middle of the stable and the fluctuating columns. Similar to Yang et al. (2017), toluene concentrations decreased at a faster pace at first, but after multiple saturation cycles, toluene concentrations showed a steady state condition. Moreover, the concentration increase could be the results of dissolutions which known as the main cause for mass transfer at a pore scale level (Vasudevan et al. 2015). Therefore, toluene in both dissolved and free phase, would be carried by hydrodynamic forces which caused by WTF (Sookhak Lari et al. 2019; Yang et al. 2017). At the bottom of S1, no toluene was detected, while toluene concentrations in F1 increased when water level falls and decreased when water level rises.

In high salinity columns (i.e., S2 and F2), the initial toluene concentrations at the top, middle, and bottom of the columns were 52, 186, and 0 mg L<sup>-1</sup> and 83, 105 and 0 mg L<sup>-1</sup>, respectively. Similar to the low salinity columns, the concentration of toluene was the highest at the middle of the

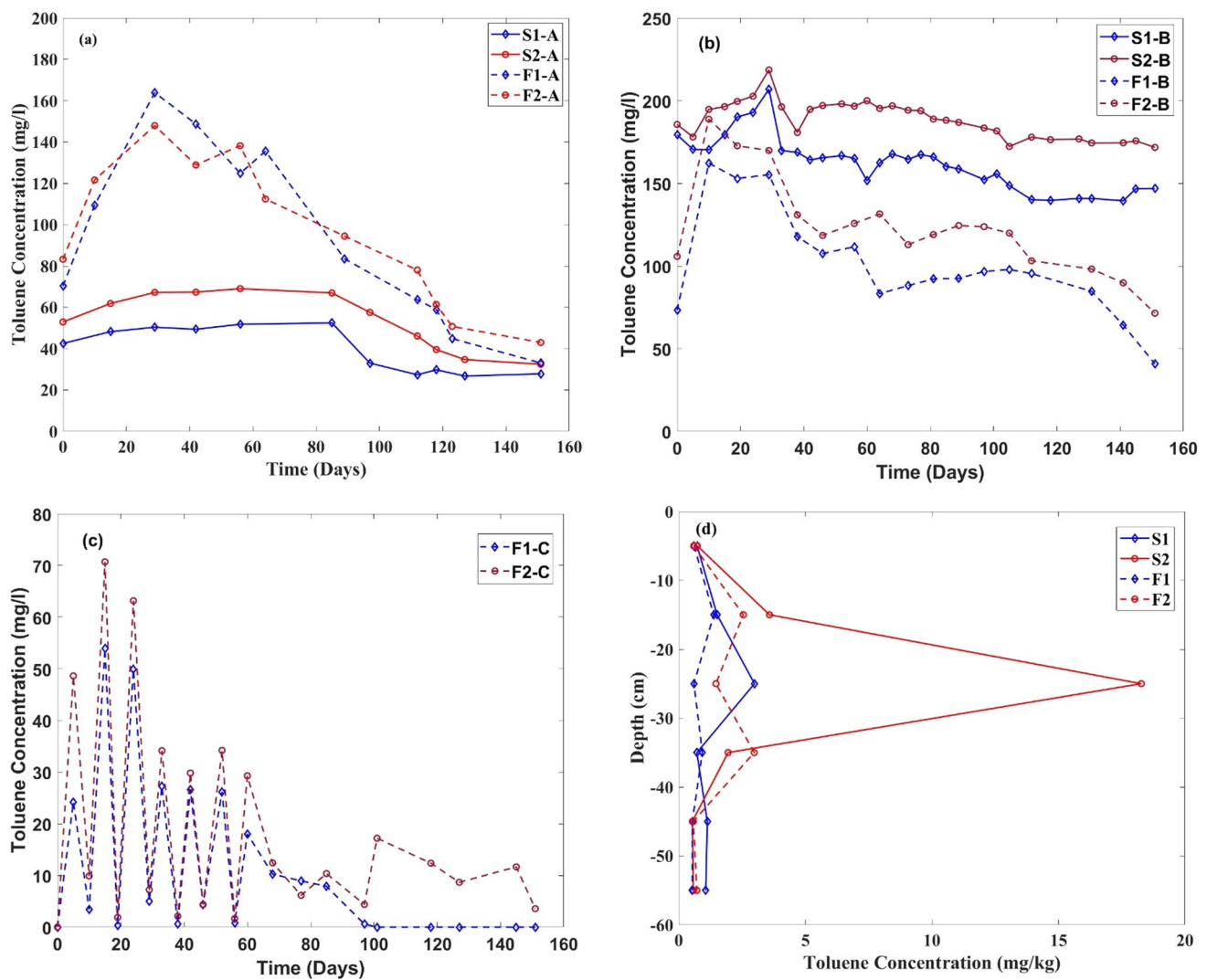


**Fig. 7** Toluene concentrations for **a** depth A, **b** for depth B, **c** for depth C, and **d** for final soil concentrations of the columns S1, S2, F1, and F2

columns. For the top of S2 and F2 ( $p$  value = 0.0078 < 0.05). At the top of column S2, slight change was observed in toluene concentration at ~80 days. In F2, toluene concentrations increased to a maximum value of 150 mg L<sup>-1</sup> by the third saturation cycle. Thereafter, the concentration decreased until it reached 42 mg L<sup>-1</sup>. At the middle of S2, the concentration increased to a maximum value of 220 mg L<sup>-1</sup> after 29 days, whereas in F2, a maximum concentration of 170 mg L<sup>-1</sup> was reached after 10 days (i.e., the second saturation cycle). Similar to the observation in the low salinity experiments, at the bottom of S2, no toluene was detected at the bottom of the S2, whereas in the case of F2, toluene concentrations decreased when water level rise and increased when water level dropped. Since diffusion was the only mass transfer mechanism in stable columns, no toluene was observed at the bottom of these columns during the lifetime of the experiments. This is consistent with the observations

of Werner and Höhener (2002). As can be seen that WTF enhanced mass transfer of dissolved toluene vertically in the column (Lee et al. 2001a, b; Dobson et al. 2007; Alazaiza et al. 2020), which, as a result of higher flow rates, would lead to more dissolution in the columns (Teramoto and Chang 2017).

To investigate the impact of salinity on a certain water level regime, S1 was compared to S2 and F1 was compared to F2. In stable water level conditions (i.e., S1 and S2), high toluene concentrations were observed in S2. At the top of S1 and S2 ( $p$  values = 0.0165 < 0.05), there was no significant change in concentrations in the first 80 days, followed by small decrease occurred between 100 and 150 days. The toluene that was pushed up in the stable column as a result of sampling remained there for the remainder of the experiment with no apparent decrease. In a natural setting groundwater that would result in continuous source of

groundwater contamination (Al-Raoush 2009; Kehew and Lynch 2011; Ning et al. 2018). Whereas in the middle of S1 and S2, toluene concentrations increased to its maximum of 200 and 220 mg L<sup>-1</sup>, respectively, at 29 days, then fluctuated between 200 to 150 mg L<sup>-1</sup> until the end of the experiment. The increase in toluene concentration can be attributed to the increased of contact time between water and toluene which may results in toluene to be slowly dissolved. This observation can be supported by decrease in EC concentrations which was observed in middle of S1 (Figure A 1). The dissolution of LNAPLs can reduce the ionic strength of groundwater (Vincent et al. 2011). Slight differences in concentrations between the two columns were observed.

For the fluctuating columns (i.e., F1 and F2), toluene concentrations followed the same trend, where F2 has higher concentrations at all depths. At the top of columns ( $p$  values = 0.9215 > 0.05), toluene concentrations in both columns increased by the third saturation cycle, then dropped, whereas in the middle of the columns, the concentrations increased to its maximum by the second saturation cycle, then decreased drastically by 40 and 60 days which corresponds to the drastic change in ORP (Fig. 4). The decrease in toluene concentration corresponds to ORP reduction and the enhancement of the anaerobic condition can be attributed to the biodegradation process. Moreover, an increase in pH values were notices during the experiment and alkaline conditions were attained in F1 and F2 by the end of the experiment (Figure A 2) which can be attributed to the addition of some salts and ions which introduced to the system due to the mineralization of toluene (Shafieiyoun et al. 2020a, b; Vincent et al. 2011). A subsequent increase of EC values is attributed to the enhancement of biodegradation due to the increase of total dissolved solids (Lopes de Castro and Branco 2003).

The bottom of the columns F1 and F2 ( $p$  values = 0.0501 > 0.05) had the same pattern of increasing and decreasing with the saturation and drainage cycles. It is expected that toluene was redistributed in the columns by advective mass transfer due to the fluctuation of water table (Balseiro-Romero et al. 2018). For the column F1, the toluene completely depleted after 100 days from the beginning of the experiment, while for the column F2, the toluene concentration reached 3 mg L<sup>-1</sup> by the end of the experiment.

Overall, it can be concluded that the concentration of toluene decreased by an average of 83%, 74%, 38%, and 37% in columns F1, F2, S1, and S2, respectively. In general, the concentration reduction was observed to be higher in the columns F1 and F2 as compared to the columns S1 and S2. In terms of salinity, the decrease in toluene concentration was higher in F1 than F2, and slightly in S1 than S2. These results support the conclusion that WTF has superiority effect over salinity when it comes to dissolution and degradation of toluene.

The behavior of toluene at the top of S1 was different than the top of F1, where toluene moved up in S1 with no change in concentration, whereas in F1, the concentration of toluene increased and reached a maximum concentration, and then decreased by 69%. At the middle of S1 and F1, for S1, toluene concentration reached its maximum after 29 days, while for F1 after 10 days. Toluene concentration for S1 decreased slightly, while for F1 decreased rapidly. At the bottom of S1, toluene was not observed, while for F1, toluene concentration increased and decreased with the WTF. Same pattern occurred between S2 and F2 at the top where at F2 toluene increased and reached a maximum concentration then decreased by 57%. For the middle of S2 and F2, for S2, toluene concentration reached its maximum after 29 days, while F2 after 10 days, with rapid decrease at F2. Similar observations applied to the bottom of S2 and F2.

Upon the completion of the experiments, the solid-phase concentration of toluene in the soil was measured by GC–MS. Figure 7d shows toluene concentrations in the soil at different depths for all soil columns. For the low salinity columns (i.e., S1 and F1), a maximum concentration of 3 mg kg was detected in S1 between – 20 and – 30 cm, whereas for the F1, the highest concentration was 1.4 mg kg<sup>-1</sup> was detected between – 10 and – 20 cm. For the high salinity columns, (i.e., S2 and F2), a maximum toluene concentration of 18 mg kg was observed in S2 between – 20 and – 30 cm, whereas in F2, a maximum concentration of 3 mg kg was detected between – 30 to – 40 cm. The highest toluene concentrations were observed in the stable columns compared with the fluctuating columns. In stable columns, the highest concentration of toluene was observed between – 20 and – 30 cm where toluene was injected. For the column S1, toluene concentration was observed between – 40 and – 50 cm, while for S2 no toluene was observed. This can be explained by the higher salinity inhibited toluene diffusion downward (Xie et al. 1997), which explain the peak concentrations at the middle of S2. For the fluctuating columns (i.e., F1 and F2), the higher concentration of toluene was observed between – 10 to – 20 cm for the column F2. It can be concluded that for columns S1 and S2, the concentration of toluene in the soil along the column is 68% higher in S2, the same goes for the columns F1 and F2, the concentration of toluene along the column F2 is 48% higher than F1. It can be summarized that the fluctuating columns have less toluene concentrations as compared to the stable columns.

### Concentration of dissolved and solid-phase benzene

Dissolved benzene concentration for all soil columns is presented in Fig. 8a–c. Benzene known for having a higher dissolving rate than any of the other BTEX chemicals (Njobuenwu et al. 2005). For the low salinity columns (i.e., S1 and F1), the initial benzene concentrations in S1 were



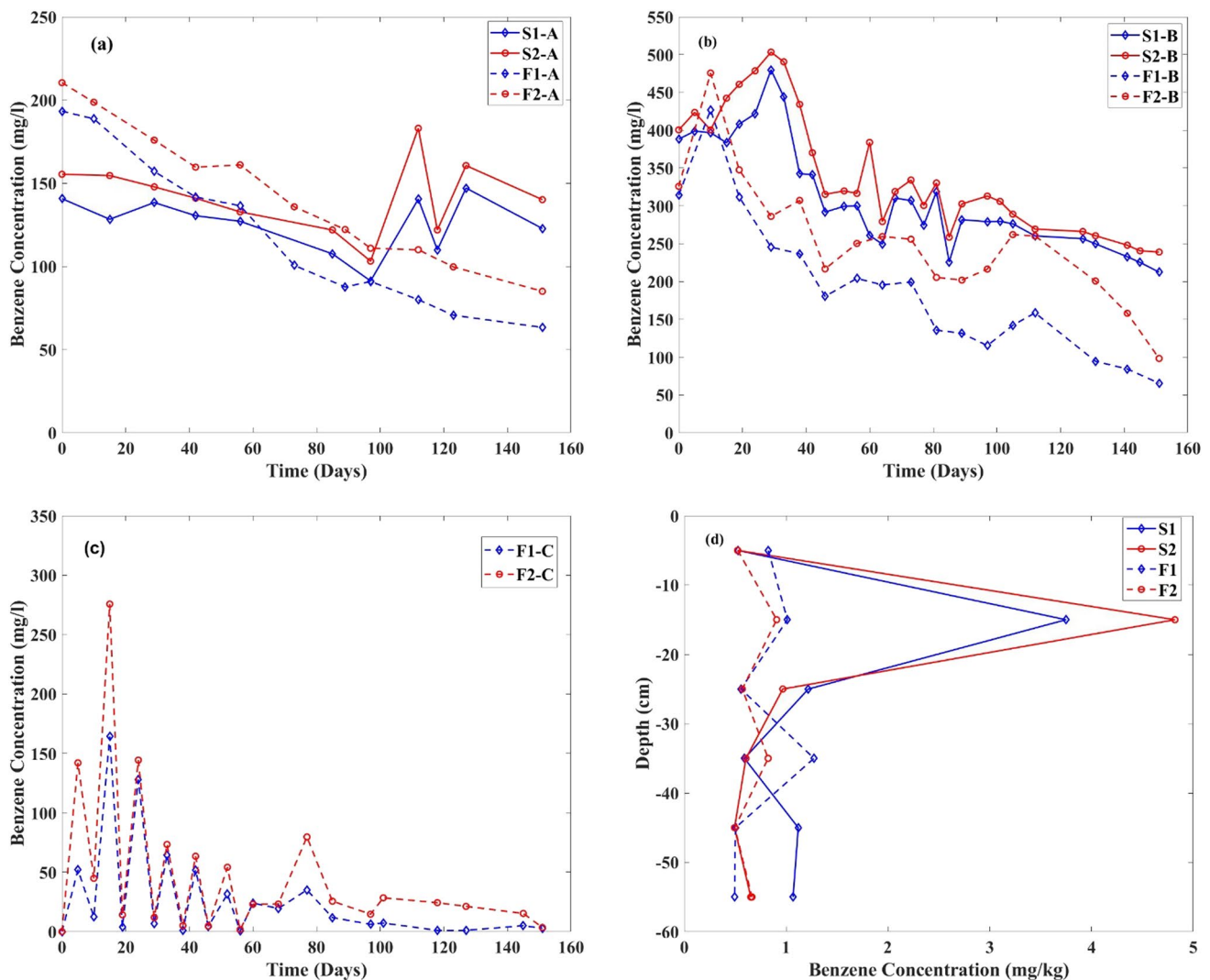


**Fig. 8** Benzene concentrations for **a** depth A, **b** depth B, **c** depth C, and **d** the final benzene concentration of the stable and fluctuating water table columns S1, S2, F1, and F2

140, ~400, and 0 mg L<sup>-1</sup> at the top, middle, and bottom (Fig. 8a–c), respectively. While the concentrations in F1 were 190, 300, and 0 mg L<sup>-1</sup> at the top, middle, and bottom, respectively. The concentration of benzene was highest at the middle of the columns, where the middle of the column is considered as a source zone of the LNAPL. For the top of S1 and F1 ( $p$  value = 0.5327 > 0.05), a slight decrease was observed in benzene concentration at the first 100 days in S1, while after that, concentration fluctuated until the end of the experiment. For F1, benzene concentrations decreased gradually to reach 60 mg L<sup>-1</sup> by end of the experiment. In the middle of S1, benzene concentration increased to a maximum value of 480 mg L<sup>-1</sup> after 29 days, while for F1, it reached its maximum concentration of 430 mg L<sup>-1</sup> after 10 days (i.e., the second saturation cycle). The statistical analysis test for the concentrations of benzene at the middle

of all columns showed that there are statistical differences ( $p$  value  $9.58 \times 10^{-7} < 0.05$ ). At the bottom of S1, no benzene was detected, while for F1, benzene concentrations increased when WT falls and decreased when WT rises.

For the high salinity columns (i.e., S2 and F2), the initial benzene concentrations in S2 were 150, 400, and 0 mg L<sup>-1</sup> at the top, middle, and bottom, respectively. On the other hand, the concentrations in F2 were 210, 300, and 0 mg L<sup>-1</sup> at the top, middle, and bottom, respectively. At the top of the columns S2 and F2 ( $p$  value = 0.9738 > 0.05), similar to S1, a small decline in benzene concentration was seen during the first 100 days, followed by concentration variation till the completion of the experiment. For the column F2, benzene concentrations decreased gradually to reach 100 mg L<sup>-1</sup> by end of the experiment. In the middle of S2, benzene concentration increased to a maximum value of



500 mg L<sup>-1</sup> after 29 days, while for F2, it reached its maximum concentration of 480 mg L<sup>-1</sup> after 10 days following benzene injection (i.e., the second saturation cycle). At the bottom of the column S2, no benzene was detected, while for F2, benzene concentrations increased when WT rises and decreased when WT moves down. Higher concentrations of benzene were observed in the stable and fluctuating columns as compared to toluene due to its higher solubility in water (1780 mg L<sup>-1</sup>). Similar to toluene, benzene was distributed along the soil column due to water table fluctuations, and higher concentrations were observed in stable columns as compared to the fluctuating columns at the source zone.

To investigate the impact of salinity on a certain water level regime, S1 was compared to S2 and F1 was compared to F2. At the top of S1 and S2 ( $p$  value = 0.0818 > 0.05), both columns followed the same pattern with slight increase observed in benzene concentrations in S2. It was observed that, the behavior of benzene in the stable water columns was different than toluene as the concentrations were measured at the top of the stable columns are close in value to the fluctuating columns. This observation can be attributed to the higher benzene solubility rate as compared to toluene. A small decrease in benzene concentration has been observed as benzene can only be diffused down or volatilised in the upper part of the column. At the middle of S1 and S2, the concentration of benzene increases to its maximum value after 29 days following the injection. As explained before, the increase in benzene concentration can be attributed to the dissolution of the entrapped benzene. Dobson et al. (2007) stated that when LNAPLs are entrapped below the WT, an isolated blob (or ganglia) of LNAPL will increase the interfacial area between the LNAPL and water, hence, encouraging accelerated LNAPL dissolution. The decrease in ORP at this section of the column, which is associated with a decrease in sulfate concentrations and a rise in DIC and EC, can be attributed to benzene degradation by SBR, which occurred in two experiments utilized soil from the same location and under similar experimental conditions. (Ngueleu et al. 2019; Shafieiyoun et al. 2020a, b).

No benzene was observed at the bottom of the stable columns. For the fluctuated columns (i.e., F1 and F2), at the top of the columns F1 and F2 ( $p$  value = 0.1783 > 0.05), benzene concentrations decreased gradually as a result of the water table fluctuation between the top of the columns and - 40 cm, benzene moved down during drainage cycle, thus, the concentration of benzene decreased gradually at the top of the columns and reached a concentration of 60 and 80 mg L<sup>-1</sup> by the end of the experiment for F1 and F2, respectively. Benzene concentration at the middle of F1 and F2 increased to its maximum at the second imbibition cycle, as a result of increase dissolution of benzene (Dobson et al. 2007). At 40 days following the injection of benzene, its concentration decreased to 65 and 100 mg L<sup>-1</sup> for F1 and

F2, respectively. The decrease in pore water benzene concentration at the middle of F1 and F2 for the whole experiment reached 82% and 78%, respectively. At the bottom of the columns F1 and F2 ( $p$  value = 0.0826 > 0.05), same observation was made, at each drainage cycle, the concentration of benzene was increased suggesting that benzene moved downward when WT moves down. The concentration continued to be fluctuated with each drainage and saturated cycle until it reached ~ 3 mg L<sup>-1</sup> for both columns by the end of the experiment. Overall, it can be concluded that the pore water concentration of benzene decreased by an average of 82%, 78%, 35%, and 32% for the columns F1, F2, S1, and S2, respectively. For the stable columns (i.e., S1 and S2), benzene moved to the top of the column due to sampling and stayed there. The concentration was gradually reduced throughout the experiment until 100 days, when it fluctuated till the end. The middle of the stable column (i.e., S1 and S2) has the highest benzene concentration relative to the top since it is the source zone, whereas benzene didn't move to the bottom of the column as diffusion occurred slowly. The concentration of benzene at the top and middle of S2 are higher than S1, which can be explained by the higher salinity that affected the dissolution and natural attenuation of benzene. The behavior of benzene at the top of S1 differs from that of F1, where S1 has little change in concentration but F1 has a 68% decline in concentration throughout the experiment. At the middle of S1 and F1, benzene concentration reached its maximum after 29 days and 10 days, respectively. No benzene has been observed at the bottom of S1, while the concentration increased and decreased with the WTF at F1. Same pattern between S2 and F2 was observed, where benzene moved up in S2 with no obvious change in concentration, whereas in F2, it declined by 62%. For the middle of S2 and F2, benzene concentration reached its maximum after 29 days, and 10 days, respectively where the concentration at S2 decreased slightly, while for F2 decreased rapidly. Although the degradation of BTEX was studied by Johnson et al. (2003) under a variety of redox settings, the degradation of benzene was only linked to the decrease in sulfate concentrations.

Figure 8d shows the concentration of benzene in the soil at different depths which was measured by GC-MS. The maximum benzene concentrations for the low salinity columns (i.e., S1 and F1), were 4 and 1.3 mg kg, respectively, between - 10 to - 20 cm for S1, and between - 30 to - 40 cm for F1. The maximum benzene concentrations for the high salinity columns (i.e., S2 and F2), were 5 and 0.9 mg kg, respectively, between - 10 to - 20 cm for S2, and between - 30 to - 40 cm for F2. Ngueleu et al. (2018) measured the sorption of benzene in two different salinities and he found that with increase salinity the adsorption of benzene tends to increase. But the superiority of water table fluctuations in F2 decrease the adsorption.

The following conclusions can be drawn from a comparison of the stable and fluctuating water level columns: firstly, the concentration of benzene and toluene for stable columns decreased slightly during the experiments, while for fluctuating columns benzene concentration decreased significantly. Secondly, the fluctuating WT within the capillary fringe resulted in the increase of the aqueous phase concentration and consequently decreases the free phase LNAPLs which resulted in more mass removal (Kemblowski and Chiang 1990; Dobson et al. 2007). Thirdly, the low initial aqueous phase concentration for both toluene and benzene at the start of the experiment, reached their maximum solubility at the source zone after 10 days for F1 and F2, and after 29 days for S1 and S2. This conclusion suggests that WTF enhance dissolution of LNAPLs, and thus the natural attenuation (Dobson et al. 2007). Moreover, the degradation of petroleum hydrocarbon can be optimized by isolating the degrading bacteria and optimizing the conditions influencing biodegradation process such as the soil pH, nutrients, and temperatures as in the case of Farahani and Mahmoudi (2018).

## Conclusion

Natural attenuation in LNAPLs contaminated groundwater is greatly affected by the movement of water table. Fluctuations of the water table within LNAPL-contaminated subsurface environments induce changes LNAPLs source zone and the geochemical properties of soil and groundwater. Results showed that redox conditions were not constant but fluctuated spatially and temporally in the soil columns. ORP values at the middle of the fluctuating columns in the case of the low and high salinity behaves differently than the middle of the stable columns and the salinity has no effects on ORP values. The differences in ORP behavior were due to the presence of organics and the changing WT level in this area. The aqueous phase of iron, manganese, nitrogen, and nitrate were detected in the system in very low concentrations; however, sulfur was plentiful, making it the major electron acceptor. The soluble components of benzene and toluene were depleted faster in the fluctuating columns, resulting in a shorter lifespan for the source zone. The hydrogeochemical indicators ORP, EC, pH, and sulfate concentrations indicated that biodegradation occur in the columns. Pore water toluene decreased by an average of 83%, 74%, 38%, and 37% for the columns F1, F2, S1, and S2, respectively. While pore water benzene decreased by an average of 82%, 78%, 35%, and 32% for the columns F1, F2, S1, and S2, respectively. The natural attenuation was also improved for the columns F1 and F2, as seen by the consumption of sulfate as compared to the columns S1 and S2. In spite of a variety of factors, including site-specific ones, results of this study showed that

WTF might be used to speed up the remediation of LNAPL contaminated aquifers.

**Supplementary Information** The online version contains supplementary material available at <https://doi.org/10.1007/s12665-023-11051-6>.

**Acknowledgements** This study was funded by NPRP Grant #NPRP9-93-1-021 from the Qatar national research fund (a member of Qatar Foundation). Findings achieved herein are solely the responsibility of the authors. We acknowledge that all the gas chromatography and dissolved inorganic/organic carbon (DIC/DOC) concentrations analyses were conducted in the Central Laboratories unit, Qatar University. We are thankful to Khaled A. Al-Jaml, Ahmad A. Ahmadi and Dr. Ahmed Abdelsalam for their valuable assistance during the experiments and sample analyses.

**Author contributions** R.I.: methodology, investigation, formal analysis, and writing—original draft, R.A.: methodology, conceptualization, investigation, supervision, writing—review and editing, funding acquisition, resources, M.A: writing—review and editing

**Funding** Open Access funding provided by the Qatar National Library. Funding was supported by Qatar Foundation (Grant # NPRP9-93-1-021).

**Data availability** The datasets generated during and/or analyzed during the current study are available from the corresponding author on reasonable request.

## Declarations

**Conflict of interest** The authors declare that they have no conflict of interest.

**Open Access** This article is licensed under a Creative Commons Attribution 4.0 International License, which permits use, sharing, adaptation, distribution and reproduction in any medium or format, as long as you give appropriate credit to the original author(s) and the source, provide a link to the Creative Commons licence, and indicate if changes were made. The images or other third party material in this article are included in the article's Creative Commons licence, unless indicated otherwise in a credit line to the material. If material is not included in the article's Creative Commons licence and your intended use is not permitted by statutory regulation or exceeds the permitted use, you will need to obtain permission directly from the copyright holder. To view a copy of this licence, visit <http://creativecommons.org/licenses/by/4.0/>.

## References

- Abbas M, Jardani A, Ahmed AS, Revil A, Brigaud L, Bégassat P, Dupont JP (2017) Redox potential distribution of an organic-rich contaminated site obtained by the inversion of self-potential data. *J Hydrol* 554:111–127
- Alazaiza MYD, Ngien SK, Copty N, Bob MM, Kamaruddin SA (2019) Assessing the influence of infiltration on the migration of light non-aqueous phase liquid in double-porosity soil media using a light transmission visualization method. *Hydrogeol J*. <https://doi.org/10.1007/s10040-018-1904-1>
- Alazaiza MYD, Ramli MH, Copty NK, Sheng TJ, Aburas MM (2020) LNAPL saturation distribution under the influence of water table fluctuations using simplified image analysis method. *Bull Eng Geol Environ* 79(3):1543–1554. <https://doi.org/10.1007/s10064-019-01655-3>

- Al-Ghouti MA, Al-Kaabi MA, Ashfaq MY, Dana DA (2019) Produced water characteristics, treatment and reuse: a review. *J Water Process Eng* 28(January):222–239. <https://doi.org/10.1016/j.jwpe.2019.02.001>
- Al-Raoush RI (2009) Impact of wettability on pore-scale characteristics of residual nonaqueous phase liquids. *Environ Sci Technol* 43(13):4796–4801. <https://doi.org/10.1021/es802566s>
- Al-Raoush RI (2014) Experimental investigation of the influence of grain geometry on residual NAPL using synchrotron microtomography. *J Contam Hydrol* 159:1–10. <https://doi.org/10.1016/j.jconhyd.2014.01.008>
- Anneser B, Einsiedl F, Meckenstock RU, Richters L, Wisotzky F, Griebler C (2008) High-resolution monitoring of biogeochemical gradients in a tar oil-contaminated aquifer. *Appl Geochem* 23(6):1715–1730. <https://doi.org/10.1016/j.apgeochem.2008.02.003>
- Baalousha HM (2016) Groundwater vulnerability mapping of Qatar aquifers. *J Afr Earth Sci* 124:75–93. <https://doi.org/10.1016/j.jafresci.2016.09.017>
- Balseiro-Romero M, Monterroso C, Casares JJ (2018) Environmental fate of petroleum hydrocarbons in soil: review of multiphase transport, mass transfer, and natural attenuation processes. *Pedosphere* 28(6):833–847
- Borch T, Kretzschmar R, Skappler A, Van Cappellen P, Ginder-Vogel M, Voegelin A, Campbell K (2010) Biogeochemical redox processes and their impact on contaminant dynamics. *Environ Sci Technol* 44(1):15–23. <https://doi.org/10.1021/es9026248>
- Cavelan A, Gol F, Colombano S, Davarzani H, Deparis J, Faure P (2022) A critical review of the influence of groundwater level fluctuations and temperature on LNAPL contaminations in the context of climate change. *Sci Total Environ*. <https://doi.org/10.1016/j.scitotenv.2021.150412>
- Chapelle FH, Bradley PM, Lovley DR, Vroblesky DA (1996) Measuring rates of biodegradation in a contaminated aquifer using field and laboratory methods. *Ground Water* 34(4):691–698. <https://doi.org/10.1111/j.1745-6584.1996.tb02057.x>
- Chen M, Al-Maktoumi A, Al-Mamari H, Izady A, Reza Nikoo M, Al-Busaidi H (2020) Oxygenation of aquifers with fluctuating water table: a laboratory and modeling study. *J Hydrol*. <https://doi.org/10.1016/j.jhydrol.2020.125261>
- Davis GB, Barber C, Power TR, Thierrin J, Patterson BM, Rayner JL, Wu Q (1999) The variability and intrinsic remediation of a BTEX plume in anaerobic sulphate-rich groundwater. *J Contam Hydrol* 36(3–4):265–290. [https://doi.org/10.1016/S0169-7722\(98\)00148-X](https://doi.org/10.1016/S0169-7722(98)00148-X)
- Dobson R, Schroth MH, Zeyer J (2007) Effect of water-table fluctuation on dissolution and biodegradation of a multi-component, light nonaqueous-phase liquid. *J Contam Hydrol* 94(3–4):235–248. <https://doi.org/10.1016/j.jconhyd.2007.07.007>
- Ebrahimi F, Lenhard RJ, Nakhaei M, Nassery HR (2019) An approach to optimize the location of LNAPL recovery wells using the concept of a LNAPL specific yield. *Environ Sci Pollut Res* 26(28):28714–28724. <https://doi.org/10.1007/s11356-019-06052-7>
- Farahani M, Mahmoudi D (2018) Optimization, modeling and its conformity with the reality of physico-chemical and microbial processes of petroleum hydrocarbons reduction in soil: a case study of Tehran oil refinery. *Environ Earth Sci* 77(9):329
- Feisthauer S, Seidel M, Bombach P, Traube S, Knöller K, Wange M, Fachmann S, Richnow HH (2012) Characterization of the relationship between microbial degradation processes at a hydrocarbon contaminated site using isotopic methods. *J Contam Hydrol* 133:17–29
- Foght J (2008) Anaerobic biodegradation of aromatic hydrocarbons: pathways and prospects. *Microb Physiol* 15(2–3):93–120
- Greskowiak J, Prommer H, Massmann G, Johnston CD, Nützmann G, Pekdeger A (2005) The impact of variably saturated conditions on hydrogeochemical changes during artificial recharge of groundwater. *Appl Geochem* 20(7):1409–1426
- Gupta P, Yadav B (2017) Bioremediation of nonaqueous phase liquids (NAPLs)-polluted soil–water resources. *Environ Pollut Bioremediat Approaches*. <https://doi.org/10.1201/9781315173351-9>
- Gupta PK, Yadav B, Yadav BK (2019) Assessment of LNAPL in subsurface under fluctuating groundwater table using 2D sand tank experiments. *J Environ Eng* 145(9):04019048. [https://doi.org/10.1061/\(asce\)ee.1943-7870.0001560](https://doi.org/10.1061/(asce)ee.1943-7870.0001560)
- Gupta PK, Yadav BK (2020) Three-dimensional laboratory experiments on fate and transport of LNAPL under varying groundwater flow conditions. *J Environ Eng* 146(4):04020010
- Haberer CM, Rolle M, Cirpka OA, Grathwohl P (2012) Oxygen transfer in a fluctuating capillary fringe. *Vadose Zone Journal* 11(3):vzj2011.0056. <https://doi.org/10.2136/vzj2011.0056>
- Hatipoğlu-Bağcı Z, Motz LH (2019) Methods for investigation of natural attenuation and modeling of petroleum hydrocarbon contamination in coastal aquifers. *Geol Eng J/Jeoloji Mühendisliği Dergisi* 43(1):131–154
- Huang WH, Asce SM, Kao CM, Asce F (2016) Bioremediation of petroleum-hydrocarbon contaminated groundwater under sulfate-reducing conditions: effectiveness and mechanism study. *J Environ Eng* 142(3):04015089. [https://doi.org/10.1061/\(asce\)ee.1943-7870.0001055](https://doi.org/10.1061/(asce)ee.1943-7870.0001055)
- Huang X, Liu G, Xia C, Yang M (2021) Simulated groundwater dynamics and solute transport in a coastal phreatic aquifer subjected to different tides. *Mar Georesour Geotechnol* 39(6):719–734. <https://doi.org/10.1080/1064119X.2020.1754975>
- Ismail R, Shafieiyou S, Al-Raoush RI (2020) Influence of water table fluctuation on natural source zone depletion in hydrocarbon contaminated subsurface environments. <https://qspace.qu.edu.qa/handle/10576/14643>
- Jeong J, Charbeneau RJ (2014) An analytical model for predicting LNAPL distribution and recovery from multi-layered soils. *J Contam Hydrol* 156:52–61. <https://doi.org/10.1016/j.jconhyd.2013.09.008>
- Jia M, Bian X, Yuan S (2017) Production of hydroxyl radicals from Fe(II) oxygenation induced by groundwater table fluctuations in a sand column. *Sci Total Environ* 584–585:41–47. <https://doi.org/10.1016/j.scitotenv.2017.01.142>
- Johnson SJ, Woolhouse KJ, Prommer H, Barry DA, Christofi N (2003) Contribution of anaerobic microbial activity to natural attenuation of benzene in groundwater. *Eng Geol* 70(3–4):343–349
- Kehew AE, Lynch PM (2011) Concentration trends and water-level fluctuations at underground storage tank sites. *Environ Earth Sci* 62(5):985–998. <https://doi.org/10.1007/s12665-010-0583-6>
- Kemblowski MW, Chiang CY (1990) Hydrocarbon thickness fluctuations in monitoring wells. *Groundwater* 28(2):244–252. <https://doi.org/10.1111/j.1745-6584.1990.tb02252.x>
- Khan MAI, Biswas B, Smith E, Naidu R, Megharaj M (2018) Toxicity assessment of fresh and weathered petroleum hydrocarbons in contaminated soil—a review. *Chemosphere*. <https://doi.org/10.1016/j.chemosphere.2018.08.094>
- Laverman AM, Pallud C, Abell J, Cappellen PV (2012) Comparative survey of potential nitrate and sulfate reduction rates in aquatic sediments. *Geochim Cosmochim Acta* 77:474–488. <https://doi.org/10.1016/j.gca.2011.10.033>
- Lee BC, Lee J, Cheon J, Lee K (2001a) Attenuation of petroleum hydrocarbons in smear zones: a case study. *J Environ Eng* 127:639–647. [https://doi.org/10.1061/\(asce\)0733-9372\(2001\)127:7\(639\)](https://doi.org/10.1061/(asce)0733-9372(2001)127:7(639))
- Lee JY, Cheon JY, Lee KK, Lee SY, Lee MH (2001b) Factors affecting the distribution of hydrocarbon contaminants and



- hydrogeochemical parameters in a shallow sand aquifer. *J Contam Hydrol* 50(1–2):139–158. [https://doi.org/10.1016/S0169-7722\(01\)00101-2](https://doi.org/10.1016/S0169-7722(01)00101-2)
- Logeshwaran P, Megharaj M, Chadalavada S, Bowman M, Naidu R (2018) Petroleum hydrocarbons (PH) in groundwater aquifers: An overview of environmental fate, toxicity, microbial degradation and risk-based remediation approaches. *Environ Technol Innov* 10:175–193. <https://doi.org/10.1016/j.eti.2018.02.001>
- Lopes de Castro D, Branco RMGC (2003) 4-D ground penetrating radar monitoring of a hydrocarbon leakage site in Fortaleza (Brazil) during its remediation process: a case history. *J Appl Geophys* 54(1–2):127–144. <https://doi.org/10.1016/j.jappgeo.2003.08.021>
- Lueders T (2017) The ecology of anaerobic degraders of BTEX hydrocarbons in aquifers. *FEMS Microbiol Ecol* 93(1):1–13. <https://doi.org/10.1093/femsec/fiw220>
- Mahmoudi D, Rezaei M, Ashjari J, Salehghamari E, Jazaei F, Babakhani P (2020) Impacts of stratigraphic heterogeneity and release pathway on the transport of bacterial cells in porous media. *Sci Total Environ* 729:138804
- McMahon PB, Chapelle FH, Bradley PM (2011) Evolution of redox processes in groundwater. *ACS Symp Ser* 1071(January):581–597. <https://doi.org/10.1021/bk-2011-1071.ch026>
- Meng L, Zuo R, Wang J, sheng, Li, Q., Du, C., Liu, X., and Chen, M. (2021) Response of the redox species and indigenous microbial community to seasonal groundwater fluctuation from a typical riverbank filtration site in Northeast China. *Ecol Eng* 159(October 2020):106099. <https://doi.org/10.1016/j.ecoleng.2020.106099>
- Müller JB, Ramos DT, Larose C, Fernandes M, Lazzarin HS, Vogel TM, Corseuil HX (2017) Combined iron and sulfate reduction biostimulation as a novel approach to enhance BTEX and PAH source-zone biodegradation in biodiesel blend-contaminated groundwater. *J Hazard Mater* 326:229–236
- Naudet V, Revil A, Rizzo E, Bottero JY, Bégassat P (2004) Groundwater redox conditions and conductivity in a contaminant plume from geoelectrical investigations. *Hydrol Earth Syst Sci* 8(1):8–22. <https://doi.org/10.5194/hess-8-8-2004>
- Ngueleu SK, Rezanezhad F, Al-Raoush RI, Van Cappellen P (2018) Sorption of benzene and naphthalene on (semi)-arid coastal soil as a function of salinity and temperature. *J Contam Hydrol* 219(May 2019):61–71. <https://doi.org/10.1016/j.jconhyd.2018.11.001>
- Ngueleu SK, Al-Raoush RI, Shafieiyoun S, Rezanezhad F, Van Cappellen P (2019) Biodegradation kinetics of benzene and naphthalene in the vadose and saturated zones of a (semi)-arid saline coastal soil environment. *Geofluids*. <https://doi.org/10.1155/2019/8124716>
- Ning Z, Zhang M, He Z, Cai P, Guo C, Wang P (2018) Spatial pattern of bacterial community diversity formed in different groundwater field corresponding to electron donors and acceptors distributions at a petroleum-contaminated site. *Water (switzerland)* 10(7):1–14. <https://doi.org/10.3390/w10070842>
- Ohio EPA (2014) Technical Report: reduction-oxidation (redox) control in Ohio's ground water quality. November. [https://epa.ohio.gov/static/Portals/28/documents/gwqcp/redox\\_ts.pdf](https://epa.ohio.gov/static/Portals/28/documents/gwqcp/redox_ts.pdf)
- Phelps CD, Young LY (1999) Anaerobic biodegradation of BTEX and gasoline in various aquatic sediments. *Biodegradation* 10:15–25
- Qin X, Tang JC, Li DS, Zhang QM (2012) Effect of salinity on the bioremediation of petroleum hydrocarbons in a saline-alkaline soil. *Lett Appl Microbiol* 55(3):210–217
- Ramesh Kumar A, Riyazuddin P (2012) Seasonal variation of redox species and redox potentials in shallow groundwater: a comparison of measured and calculated redox potentials. *J Hydrol* 444–445:187–198. <https://doi.org/10.1016/j.jhydrol.2012.04.018>
- Reddi L, Han W, Banks MK (1998) Mass loss from lnapl pools under fluctuating water. *J Environ Eng* 124(December):1171–1177. [https://doi.org/10.1061/\(ASCE\)0733-9372\(1998\)124:12\(1171\)](https://doi.org/10.1061/(ASCE)0733-9372(1998)124:12(1171))
- Reddy KR, DeLaune RD (2008) Biogeochemistry of wetlands: science and applications. CRC Press, Boca Raton. <https://doi.org/10.1201/9780203491454-22>
- Rezanezhad F, Couture RM, Kovac R, O'Connell D, Van Cappellen P (2014) Water table fluctuations and soil biogeochemistry: an experimental approach using an automated soil column system. *J Hydrol* 509:245–256. <https://doi.org/10.1016/j.jhydrol.2013.11.036>
- Ruffino B, Zanetti M (2009) Adsorption study of several hydrophobic organic contaminants on an aquifer material. *Am J Environ Sci* 5(4):507–515. <https://doi.org/10.3844/ajessp.2009.507.515>
- Rühle FA, von Netzer F, Lueders T, Stumpp C (2015) Response of transport parameters and sediment microbiota to water table fluctuations in laboratory columns. *Vadose Zone J* 14(5):vzj2014.09.0116. <https://doi.org/10.2136/vzj2014.09.0116>
- Sei A, Fathepure BZ (2009) Biodegradation of BTEX at high salinity by an enrichment culture from hypersaline sediments of Rozel Point at Great Salt Lake. *J Appl Microbiol* 107(6):2001–2008
- Shafieiyoun S, Al-Raoush RI, Ismail RE, Ngueleu SK, Rezanezhad F, Van Cappellen P (2020a) Effects of dissolved organic phase composition and salinity on the engineered sulfate application in a flow-through system. *Environ Sci Pollut Res* 27(11):11842–11854. <https://doi.org/10.1007/s11356-020-07696-6>
- Shafieiyoun S, Al-Raoush RI, Ngueleu SK, Rezanezhad F, Van Cappellen P (2020b) Enhancement of naphthalene degradation by a sequential sulfate injection scenario in a (semi)-arid coastal soil: a flow-through reactor experiment. *Water Air Soil Pollut* 231(8):1–16. <https://doi.org/10.1007/s11270-020-04725-5>
- Sherry A, Gray ND, Ditchfield AK, Aitken CM, Jones DM, Röling WFM, Hallmann C, Larter SR, Bowler BFJ, Head IM (2013) Anaerobic biodegradation of crude oil under sulphate-reducing conditions leads to only modest enrichment of recognized sulphate-reducing taxa. *Int Biodeterior Biodegradation* 81:105–113
- Sookhak Lari K, Davis GB, Rayner JL, Bastow TP, Puzon GJ (2019) Natural source zone depletion of LNAPL: a critical review supporting modelling approaches. *Water Res* 157(5):630–646. <https://doi.org/10.1016/j.watres.2019.04.001>
- Sun L, Chen Y, Jiang L, Cheng Y (2018) Numerical simulation of the effect about groundwater level fluctuation on the concentration of BTEX dissolved into source zone. In: IOP conference series: earth and environmental science (vol 111, No 1). IOP Publishing, p 012017
- Teramoto EH, Chang HK (2017) Field data and numerical simulation of btx concentration trends under water table fluctuations: example of a jet fuel-contaminated site in Brazil. *J Contam Hydrol* 198:37–47. <https://doi.org/10.1016/j.jconhyd.2017.01.002>
- Teramoto EH, Pedre MAZ, Chang HK (2020) Impact of water table fluctuations on the seasonal effectiveness of the pump-and-treat remediation in wet-dry tropical regions. *Environ Earth Sci*. <https://doi.org/10.1007/s12665-020-09182-1>
- Ulrich AC, Guigard SE, Foght JM, Semple KM, Pooley K, Armstrong JE, Biggar KW (2009) Effect of salt on aerobic biodegradation of petroleum hydrocarbons in contaminated groundwater. *Biodegradation* 20:27–38
- Vasudevan M, Kumar GS, Nambi IM (2015) Numerical studies on kinetics of sorption and dissolution and their interactions for estimating mass removal of toluene from entrapped soil pores. *Arab J Geosci* 8:6895–6910
- Van De Ven CJC, Scully KH, Frame MA, Sihota NJ, Mayer KU (2021) Impacts of water table fluctuations on actual and perceived natural source zone depletion rates. *J Contam Hydrol* 238(July 2020):103771. <https://doi.org/10.1016/j.jconhyd.2021.103771>
- Vincent AO, Felix E, Weltme MO, Ize-Iyamu OK, Daniel EE (2011) Microbial degradation and its kinetics on crude oil polluted soil. *Res J Chem Sci Sept Res J Chem Sci* 1(6):8–14. <http://isca.me/rjcs/Archives/v1/i6/02.pdf>

- Wei Y, Thomson NR, Aravena R, Marchesi M, Barker JF, Madsen EL, Kolhatkar R, Buscheck T, Hunkeler D, DeRito CM (2018) Infiltration of sulfate to enhance sulfate-reducing biodegradation of petroleum hydrocarbons. *Groundw Monit Remediat* 38(4):73–87. <https://doi.org/10.1111/gwmmr.12298>
- Werner D, Höhener P (2002) The influence of water table fluctuations on the volatilization of contaminants from groundwater. *IAHS AISH Publ* 275:213–218
- Wurgaft E, Findlay AJ, Vigderovich H, Herut B, Sivan O (2019) Sulfate reduction rates in the sediments of the Mediterranean continental shelf inferred from combined dissolved inorganic carbon and total alkalinity profiles. *Mar Chem* 211(March):64–74. <https://doi.org/10.1016/j.marchem.2019.03.004>
- Xie WH, Shiu WY, Mackay D (1997) A review of the effect of salts on the solubility of organic compounds in seawater. *Mar Environ Res* 44(4):429–444. [https://doi.org/10.1016/S0141-1136\(97\)00017-2](https://doi.org/10.1016/S0141-1136(97)00017-2)
- Yang YS, Li P, Zhang X, Li M, Lu Y, Xu B, Yu T (2017) Lab-based investigation of enhanced BTEX attenuation driven by groundwater table fluctuation. *Chemosphere* 169:678–684. <https://doi.org/10.1016/j.chemosphere.2016.11.128>
- Zhang Z, Furman A (2021) Science of the total environment soil redox dynamics under dynamic hydrologic regimes—a review. *Sci Total Environ* 763:143026. <https://doi.org/10.1016/j.scitotenv.2020.143026>
- Zheng F, Gao Y, Sun Y, Shi X, Xu H, Wu J (2015) Influence de la vitesse d'écoulement et de l'hétérogénéité spatiale sur la migration de phase liquide non aqueuse dense (DNAPL) en milieu poreux: aperçus des expériences en laboratoire et de modélisation numérique. *Hydrogeol J* 23(8):1703–1718. <https://doi.org/10.1007/s10040-015-1314-6>
- Zhou A, Zhang Y, Dong T, Lin X, Su X (2015) Response of the microbial community to seasonal groundwater level fluctuations in petroleum hydrocarbon-contaminated groundwater. *Environ Sci Pollut Res* 22(13):10094–10106. <https://doi.org/10.1007/s11356-015-4183-6>

**Publisher's Note** Springer Nature remains neutral with regard to jurisdictional claims in published maps and institutional affiliations.